Proceedings of European Wireless Conference 2014, 14-16 May 2014, Barcelona, Spain.

Orthogonal Design of Cyclic Block Filtered Multitone Modulation

Mauro Girotto and Andrea M. Tonello
Wireless and Power Line Communications Lab, University of Udine, Italy
http://www.diegm.uniud.it/tonello/wiplilab - {mauro.girotto, tonello}@uniud.it

***Abstract*—This paper deals with the orthogonal design of a cyclic block filtered multitone modulation (CB-FMT) system. CB-FMT is a filter bank modulation scheme that uses well frequency localized pulses as in FMT but the linear convolutions are replaced by circular convolutions. We derive the orthogonality conditions both in the time domain and in the frequency domain. Then, we show that such conditions can be fulfilled with a hyper-spherical parameterization of the pulse frequency components. Finally, optimal frequency localized orthogonal pulses are searched. It is shown that much higher in-band-to-out-of-band sub-channel energy is achieved for both critically sampled and non-critically sampled architectures compared to baseline solutions corresponding to either the use of a rectangular or a root-raised-cosine window in frequency. Finally, a comparison with OFDM shows that higher spectral efficiency can be provided by orthogonal CB-FMT.**

I. Introduction

The demand for high data-rate communication systems has motivated the use of a wide spectrum and the study of new spectral efficient transmission technologies. Since wide band channels can introduce severe inter-symbol interference in single carrier digital modulation systems, multicarrier modulation has been advocated as a better option to simplify the equalization task and possibly to yield higher data rates [1]. The most popular multi-carrier modulation scheme is Orthogonal Frequency Division Multiplexing (OFDM) [2]. This scheme has been adopted in several communication standards, for both wireless and wired applications, e.g., in the WLAN IEEE 802.11 [3] and in the cellular LTE standard [4]. Despite its simplicity, which translates in a straightforward discrete Fourier transform (DFT) realization, OFDM exhibits poor sub-channel frequency confinement which jeopardizes its robustness in the presence of non-idealities, as synchronization errors [5], insufficient length cyclic prefix (in frequency selective channels), high mobility (channel time variations) [6]. Furthermore, it as it exhibits poor peak-to-average power ratio characteristics [7] and improvable spectrum agility in cognitive radio applications or when Electromagnetic Compatibility (EMC) notching masks are imposed for coexistence with others systems. This has pushed the research on alternative filter bank modulation (FBM) schemes.

A FBM system uses a synthesis filter bank for transmission with possibly well frequency localized sub-channels. In particular, in Filtered Multitone (FMT) modulation a prototype pulse is used and the frequency translation is obtained via the modulation with an exponential function [8].

Another FBM scheme, where the pulse design has been analyzed, is OFDM/OQAM [9].

In this paper, we consider a FBM scheme that we refer to as Cyclic Block Filtered Multitone Modulation [10]. Similarly to FMT well localized sub-channels are used, but the linear convolutions are replaced with cyclic convolutions. We have shown that CB-FMT can be implemented in the frequency domain with a significant lower complexity than FMT with even longer pulses [11], [12]. Furthermore, it has the potentiality of yielding lower bit error rate in fading channels than OFDM and FMT thanks to the ability of exploiting frequency diversity through frequency domain equalization [10]. It can also be shown that lower peak-to-average-power ratios are obtained compared to OFDM [12].

In this paper, we focus on the orthogonal design of CB-FMT. Thanks to its cyclic convolution structure, the orthogonal pulse design is simplified compared to FMT [13], [14]. In particular, we show that both real and Hermitian complex pulses can be designed with maximum sub-channel frequency confinement. A comparison with baseline solutions corresponding to either the use of a rectangular or a root-raised-cosine window in frequency shows that improved in-band-to-out-of-band sub-channel energy is achieved for both critically sampled and non-critically sampled architectures. This can yield improved robustness of the system to channel and hardware non-idealities.

This paper is organized as follows. In Section II, we overview the CB-FMT modulation principles. In Section III, we derive the orthogonality conditions for CB-FMT in the time and the frequency domains. In Section IV, we focus on the filter bank design procedure. In Section V, we provide several design examples and we show the improvement w.r.t. baseline solutions. Finally, in Section VI, the conclusions follow.

II. Cyclic Block FMT Modulation

Cyclic Block FMT (CB-FMT) is a filter bank modulation scheme that is depicted in Fig. 1. As such, the high data-rate information signal to be transmitted is split into K low data-rate signals, denoted with $a^{(k)}(\ell N)$ with $k \in \{0, \cdots, K-1\}$. Consequently, the wide band channel is partitioned in K narrow sub-channels. The transmission takes place simultaneously modulating the low data-rate signals. To avoid interference between the sub-channels and to reduce the emissions outside the useful band, sub-channel frequency selectivity is desirable. To achieve this, the low data-rate signals are

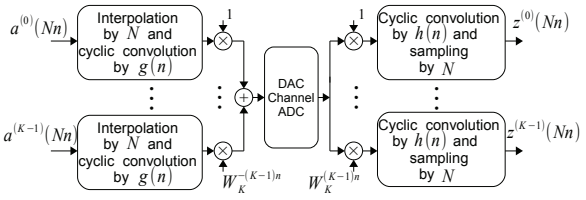

Fig. 1. Block diagram of the CB-FMT transceiver.

shaped with a frequency confined pulse. Differently from conventional filter bank modulation as FMT, the sequence of data symbols in each sub-channel is grouped into blocks of L elements. Each block is interpolated by a factor N and, then, cyclically convolved with the prototype pulse $g(n)$. The K modulated signals are translated in the frequency domain by an exponential function multiplication. Finally, the sub-channel signals are summed together to yield the transmitted signal $x(n)$. In simple formulae, this signal can be written as follows

$$\begin{aligned} x(n) &= \sum_{k=0}^{K-1} \left[a^{(k)} \otimes g\right](n) \\ &= \sum_{k=0}^{K-1}\sum_{\ell=0}^{L-1} a^{(k)}(\ell N) g((n-\ell N)_M) W_K^{-nk}, \qquad (1) \\ & n \in \{0, \cdots, M-1\}, \end{aligned}$$

where $\otimes$ denotes the circular convolution operator, $g(n)$ is the prototype pulse, $W_K^{-nk} = e^{i2\pi nk/K}$ is the complex exponential function and $(\cdot)_M = \text{mod}(\cdot, M)$ is the integer modulo operator. Differently from the linear convolution, the cyclic convolution involves periodic signals and it is performed in a period of length $M = LN$ samples. The prototype pulse $g(n)$ is a causal finite impulse response (FIR) filter of M coefficients. Without loss of generality, if the filter length is less than M, the pulse can be extended to M coefficients with zero-padding. In (1), $g((n-\ell N)_M)$ denotes the prototype pulse periodic repetition, i.e. $g((n-\ell N+kM)_M) = g(n-\ell N)$.

At the receiver, we apply a cyclic analysis filter bank to the received signal $y(n)$ using the prototype analysis pulse $h(n)$. The n-th sample associated to the k-th sub-channel can be written as

$$\begin{aligned} z^{(k)}(nN) &= \sum_{\ell=0}^{M-1} y(\ell) W_K^{\ell k} h((nN-\ell)_M), \qquad (2) \\ & k \in \{0, \ldots, K-1\}, \quad n \in \{0, \ldots, L-1\}, \end{aligned}$$

where $h((nN-\ell)_M)$ is the periodic repetition of the prototype analysis pulse.

The system processes the information data organized in K blocks of L symbols each, i.e. KL data symbols at once. The transmitted signal, derived from (1), has a duration equal to MT seconds, where T denotes the sampling period. Therefore, the transmission data rate is equal to

$$R = \frac{KL}{MT} = \frac{K}{NT} \quad \text{symbols/s.} \qquad (3)$$

CB-FMT, similarly to conventional FMT, employs frequency confined pulses. However, as explained above, the linear convolutions in FMT are replaced by cyclic convolutions. It has been shown that this yields lower implementation complexity yet using pulses with equal or higher length and using an efficient frequency domain realization [12]. In this paper, we focus on the design of an orthogonal CB-FMT system. In the next section we discuss the orthogonality conditions.

III. Orthogonality Conditions in CB-FMT

The CB-FMT system has perfect reconstruction (PR) when neither inter-symbol interference (ISI) nor inter-carrier interference (ICI) is present at the output of the analysis cyclic filter bank (assuming an ideal communication medium). To derive the PR conditions we have to combine (1) with (2). In particular, we can rearrange them to obtain

$$x(n) = \sum_{k=0}^{K-1}\sum_{\ell=0}^{L-1} \tilde{a}^{(k)}(\ell N) g^{(k)}(n-\ell N), \qquad (4)$$

$$\tilde{z}^{(h)}(mN) = \sum_{n=0}^{M-1} x(n) h^{(h)}(mN-n), \qquad (5)$$

where

$$\tilde{a}^{(k)}(\ell N) = a^{(k)}(\ell N) W_K^{-\ell N k}, \qquad (6)$$

$$\tilde{z}^{(h)}(mN) = z^{(h)}(mN) W_K^{mNh}, \qquad (7)$$

$$g^{(k)}(n) = g\left((n)_M\right) W_K^{-nk}, \qquad (8)$$

$$h^{(h)}(n) = h\left((n)_M\right) W_K^{-nh}. \qquad (9)$$

To have the circular convolution in (4) and (5), the pulses in (8) and (9) must be periodic with period M, i.e. $g^{(k)}(n+M) = g^{(k)}(n)$. This condition is valid when $Q = M/K$ is an integer number.

Now, we replace (4) into (5). After some algebraic manipulations, we obtain the following input/output relation

$$\tilde{z}^{(h)}(mN) = \sum_{k=0}^{K-1}\sum_{\ell=0}^{L-1} \tilde{a}^{(k)}(\ell N) g^{(k)} \otimes h^{(h)}(mN-\ell N). \qquad (10)$$

To proceed, we assume to have synthesis and analysis matched filters, i.e. $h(n) = g_-^*(n) = g^*(-n)$, where $(\cdot)^*$ denotes the complex conjugate operator, so that the signal-to-noise ratio (SNR), in the presence of background noise, is maximized. The relation (10) becomes

$$\tilde{z}^{(h)}(mN) = \sum_{k=0}^{K-1}\sum_{\ell=0}^{L-1} \tilde{a}^{(k)}(\ell N) r^{(k,h)}(mN-\ell N), \qquad (11)$$

$$r^{(k,h)}(mN) = g^{(k)} \otimes \left(g_-^{(h)}\right)^*(mN), \qquad (12)$$

where (12) represents the cyclic correlation between $g^{(k)}(n)$ and $g^{(h)}(n)$, sampled by a factor N.

To have orthogonality, the following two conditions must be fulfilled:

1) for $k = h$, $r^{(k,k)}(mN) = \delta_m$, where δ_m is the Kronecker delta so that no ISI is present at the output;

2) for $k \neq h$, $r^{(k,h)}(mN)$ must be always null, so that no inter-carrier (ICI) is present.

The above conditions essentially are an extension of the bi-dimensional Nyquist criterion to cyclic filter banks.

As it will be clear in Section IV, the orthogonal design of CB-FMT will be carried out in the frequency domain. Therefore, it is important to write the orthogonality conditions in the frequency domain. We start from (12) and we compute the M-point DFT to obtain

$$\begin{aligned} R^{(k,h)}(q) &= \sum_{n=0}^{L-1} r^{(k,h)}(nN) W_L^{nq} \\ &= \sum_{m=0}^{M-1} r^{(k,h)}(m)\delta_N(m) W_M^{mq}, \end{aligned} \tag{13}$$

where $\delta_N(m)$ denotes the Kronecker delta periodically repeated with period N, i.e. $\delta_N(m) = \sum_{p\in\mathbb{Z}} \delta_{m,pN}$, equal to 1 for $m \in \{pN, p \in \mathbb{Z}\}$ and 0 otherwise. The periodic delta function can be rewritten as $\delta_N(m) = \sum_{s=0}^{N-1} W_N^{ms}/N$. Substituting it in (13), we obtain

$$\begin{aligned} R^{(k,h)}(q) =& \frac{1}{N} \sum_{s=0}^{N-1} \sum_{m=0}^{M-1} r^{(k,h)}(m) W_M^{mq} W_M^{msL} \\ =& \frac{1}{N} \sum_{s=0}^{N-1} R_1^{(k,h)}(q + sL), \end{aligned} \tag{14}$$

where $R_1^{(k,h)}(q)$ is the M-point DFT of (12) before the N factor decimation. $R_1^{(k,h)}(q)$ is equal to

$$R_1^{(k,h)}(q) = G(q + kQ)G^*(q + hQ), \tag{15}$$

where $G(q)$ is M-point DFT of the prototype pulse $g((n)_M)$. Finally, substituting (15) in (14), we obtain

$$R^{(k,h)}(q) = \frac{1}{N} \sum_{s=0}^{N-1} G(q+sL+kQ)G^*(q+sL+hQ). \tag{16}$$

Finally, the orthogonality conditions can be now translated in frequency domain as follows:

1) for $k = h$, the cyclic auto-correlation of the prototype pulse must have a flat spectrum, i.e., its DFT coefficients must be equal to a constant. Analytically, the condition is expressed as

$$\begin{aligned} R^{(k,k)}(q) =& \frac{1}{N} \sum_{s=0}^{N-1} |G(q + sL + kQ)|^2 = 1, \\ & \forall q \in \{0, \ldots, L-1\}, \quad \forall k \in \{0, \ldots, K-1\}. \end{aligned} \tag{17}$$

2) for $k \neq h$, the time domain cross-correlation function $r^{(k,h)}(nN)$ must be null. Therefore, its DFT coefficients must also be null. Analytically, we have

$$\begin{aligned} \frac{1}{N} \sum_{s=0}^{N-1} G(q + sL + kQ)G^*(q + sL + hQ) = 0, \\ \forall q \in \{0, \ldots, L-1\}, \quad \forall k \in \{0, \ldots, K-1\}. \end{aligned} \tag{18}$$

In the following section, we will discuss the design of optimal orthogonal pulses.

IV. Orthogonal Pulse Design

To design an orthogonal CB-FMT system, we need to determine $G(i), i \in \{0, \ldots, M-1\}$, such that equations (17) and (18) are satisfied. The problem is non-linear and involves M variables and KL equations. We start from the condition (17). The square sum of a number of variables is equal to a constant if the variables are expressed in term of trigonometric functions. For example, a valid solution of equation $x^2 + y^2 = 1$ in $\mathbb{R}^2$ is given by $x = \cos\alpha, y = \sin\alpha$. In other words, polar coordinates solve (17) for $N = 2$, independently of the angle α. This procedure can be extended for $N = 3$ using spherical coordinates, and more generally, for $N > 3$, we can use the hyper-spherical coordinates in the $\mathbb{R}^n$ space [15]. To simplify the notation, we consider $k = 0$. So that the solution to (17) can be obtained, for $q \in \{0, \ldots, L-1\}$, as follows

$$G(q) = \sqrt{N} \cos\theta_{q,0}, \tag{19}$$

$$G(q+L) = \sqrt{N} \sin\theta_{q,0} \cos\theta_{q,1}, \tag{20}$$

$$\vdots \quad = \quad \vdots$$

$$G(q + sL)_{s\in\{2,\ldots,N-2\}} = \sqrt{N} \left(\prod_{i=0}^{s-1} \sin\theta_{q,i} \right) \cos\theta_{q,s}, \tag{21}$$

$$\vdots \quad = \quad \vdots$$

$$G(q + (N-1)L) = \sqrt{N} \left(\prod_{i=0}^{N-2} \sin\theta_{q,i} \right). \tag{22}$$

It should be noted that the DFT coefficients $\{G(q), G(q + L), \ldots, G(q+(N-1)L)\}$ are obtained from a set of $N-1$ angles, denoted as $\boldsymbol{\theta}_q = \{\theta_{q,0}, \theta_{q,1}, \ldots, \theta_{q,N-2}\}$. Thus, exploiting the angle representation, the L equations in N unknowns (17) can be rewritten as a system of L equations and $N-1$ unknown angles. If we consider a prototype pulse that is band limited, i.e. the non-zero DFT coefficients are $Q_2 < M$, the number of unknown angles is reduced. Exploiting the angles representation, these L equations are automatically verified and do not need to be solved.

To complete the orthogonal design, we need to satisfy the no-ICI condition (18). This condition is given by a non-linear system of $(K-1)L$ equations in L sets of unknown angles. To simplify the problem, the system of equations can be partitioned in disjointed sub-systems. The number of sub-systems is equal to $N_s = \gcd(Q, L)$, where $\gcd(Q, L)$ denotes the greatest common divisor between $Q = M/K$ and $L = M/N$. Each sub-system involves $N_a = L/N_s$ sets of angles and $(K-1)L/N_s$ equations. The n-th sub-system is represented as follows

$$\begin{cases} R^{(0,1)}((n + bN_s)_L) = 0 & (\boldsymbol{\theta}_{(n)_L}, \boldsymbol{\theta}_{(n+N_s)_L}) \\ R^{(0,2)}((n + bN_s)_L) = 0 & (\boldsymbol{\theta}_{(n+bN_s)_L}, \boldsymbol{\theta}_{(n+(b+2)N_s)_L}) \\ \quad\vdots & \quad\vdots \\ R^{(0,K-1)}((n + bN_s)_L) = 0 & (\boldsymbol{\theta}_{(n+bN_s)_L}, \boldsymbol{\theta}_{(n+(b+K-1)N_s)_L}) \end{cases} \tag{23}$$

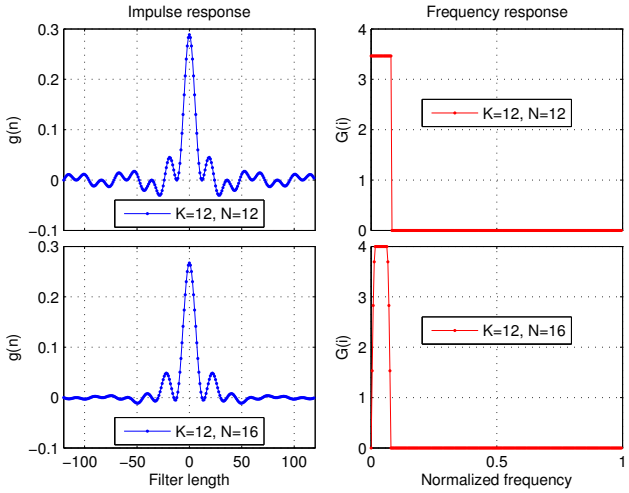

Fig. 2. Baseline prototype pulse examples for $K = 12, N = 12, M = 240$ and $K = 12, N = 16, M = 240, \beta = 0.33$. On the left, the impulse response of the base-band pulse version. On the right, frequency response (DFT coefficients).

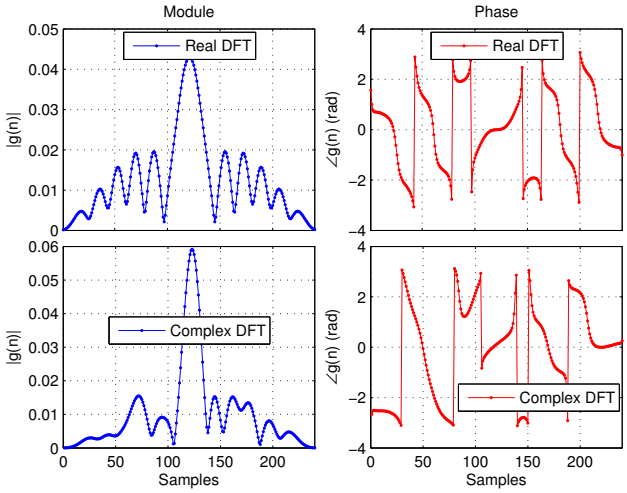

Fig. 3. Discrete impulse response of optimal prototype pulses for $K = 12, N = 16$. On the top, the real DFT coefficient pulse (Hermitian symmetry). On the bottom, the complex DFT coefficient pulse (asymmetric).

where $b \in \{0, \ldots, N_a - 1\}$ and the pair $(\boldsymbol{\theta}_a, \boldsymbol{\theta}_b)$ denotes the set of angles involved in the orthogonal condition. In the n-th sub-system of (23), there are N_a equations for each sub-channel, i.e. the $R^{(0,k)}((n + bN_s)_L)$ notation gathers the equations $R^{(0,k)}((n)_L), R^{(0,k)}((n + N_s)_L), \ldots, R^{(0,k)}((n + (N_a - 1)N_s)_L)$.

We note that the problem can be partitioned in sub-systems only if Q and L are not coprime. For example, with the parameters $K = 8, N = 10, M = 240$, we have 6 sub-systems. Each sub-system has 4 sets of angles (36 unknowns) and 28 equations. The maximum sub-system number is reached when $K = N$. In this case, we have a sub-system for each set of angles, i.e., we have L sub-systems of $N - 1$ equations in $N - 1$ unknowns.

A. Complex Solutions

Solving the system(s) in (23) as a function of angles yields real solutions, i.e., the prototype pulse M-point DFT is real. More generally, these coefficients can be complex. This suggests to modify the relations (19)-(22) to take into account the DFT coefficient phase. We, therefore, have

$$G_c(q) = G(q)e^{i\phi_{q,0}}, \tag{24}$$
$$G_c(q + L) = G(q + L)e^{i\phi_{q,1}}, \tag{25}$$
$$\vdots \quad = \quad \vdots$$
$$G_c(q + sL) = G(q + sL)e^{i\phi_{q,s}}, \tag{26}$$
$$\vdots \quad = \quad \vdots$$
$$G_c(q + (N - 1)L) = G(q + (N - 1)L)e^{i\phi_{q,N-1}}, \tag{27}$$

where $\boldsymbol{\phi}_q = \{\phi_{q,0}, \ldots, \phi_{q,N-1}\}$ are the sets of phases. Also in the complex case, the partitioning into sub-systems is possible as mentioned in Section IV. The only difference is the number of unknowns that grows from $(N - 1)L$ to $(2N - 1)L$.

B. Optimal Pulse Design

In this section, we consider the pulse design under the objective of maximizing the in-band-to-out-of-band pulse energy. This yields optimally frequency localized sub-channel pulses. The transmitted signal $x(n)$ is interpolated with an interpolation low pass filter. The objective function is defined as

$$f_m(\boldsymbol{\theta}, \boldsymbol{\phi}) = \frac{\int_0^B |G_i(f, \boldsymbol{\theta}, \boldsymbol{\phi})|^2 \, \mathrm{d}f}{\int_{-\infty}^{+\infty} |G_i(f, \boldsymbol{\theta}, \boldsymbol{\phi})|^2 \, \mathrm{d}f - \int_0^B |G_i(f, \boldsymbol{\theta}, \boldsymbol{\phi})|^2 \, \mathrm{d}f}, \tag{28}$$
$$\boldsymbol{\theta} = \{\boldsymbol{\theta}_0, \ldots, \boldsymbol{\theta}_{L-1}\},$$
$$\boldsymbol{\phi} = \{\boldsymbol{\phi}_0, \ldots, \boldsymbol{\phi}_{L-1}\},$$

where $G_i(f, \boldsymbol{\theta}, \boldsymbol{\phi})$ is the frequency response of the interpolated prototype pulse and $B = 1/KT$ is the sub-channel bandwidth. In the following numerical analysis, $x(n)$ is interpolated from the $\mathbb{Z}(T)$ discrete time domain to the $\mathbb{Z}(T/N_i)$ domain.

It should be noted that if the prototype pulse has only Q non-zero DFT coefficients, i.e. $G(i) = 0$ for $i \in \{Q, \ldots, M - 1\}$, the condition in (18) is always satisfied. A trivial orthogonal solution is to set such coefficients all equal to one. However, such a solution does not grant the maximum frequency confinement when the interpolation is taken into account. It is interesting to note that in such a case the CB-FMT system is exactly the dual of OFDM, i.e., OFDM uses a rectangular (rect) time domain window while CB-FMT uses a rectangular frequency domain window. Another possibility is to still assume only Q non zero DFT coefficients but a root-raised-cosine (rrc) window. The maximum roll-off is then chosen equal to $\beta_{MAX} = Q/L - 1$.

In the following section, we show that better than the rectangular and the rrc frequency confined pulses can be designed.

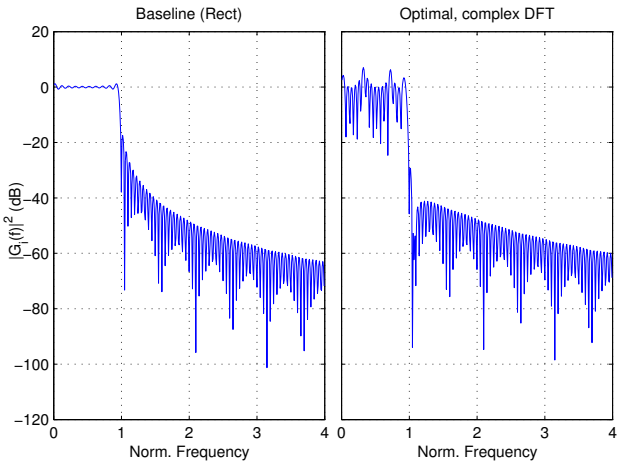

Fig. 4. Frequency response of the interpolated prototype pulses for $K = 12, N = 12$ (maximum rate). On the left, the baseline pulse: a rectangular pulse. On the right, the optimal prototype pulse with complex DFT coefficients. In this plot, the frequency is normalized to the sub-channel spacing, i.e. $1/KT = 1$.

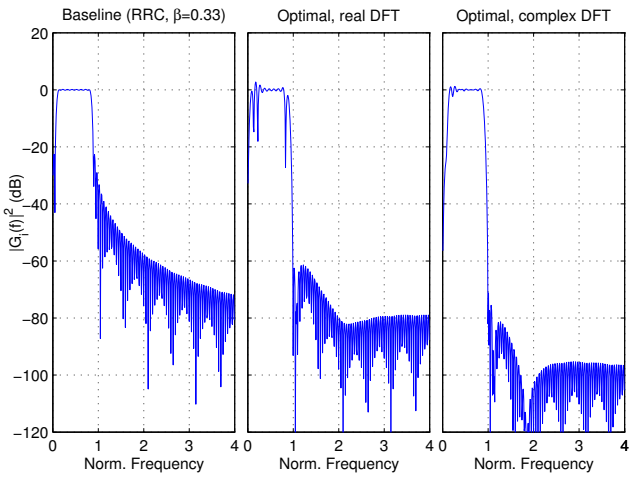

Fig. 5. Frequency response of the interpolated prototype pulses for $K = 12, N = 16$ (rate 0.75). On the left, the baseline pulse: a root-raised cosine with $\beta = 0.33$. In the middle, the optimal prototype pulse with real DFT coefficients. On the right, the optimal prototype pulse with complex DFT coefficients. In this plot, the frequency is normalized to the sub-channel spacing, i.e. $1/KT = 1$.

V. Numerical Results

We have performed a search for optimally frequency localized pulses. In particular, we consider the maximization of the objective function in (28) under the constraints in (18) with the angular parameters as in (23). The pulse is upsampled by a factor 8 and then filtered (with a linear convolution) with a 10-th order raised cosine filter. The optimization is performed exploiting the interior point method [16]–[18]. To avoid the local maximum problem, we repeat the optimization several times (starting from different and randomly initial points) and we select the pulse that offers the highest metric value.

We report results assuming a pulse length equal to $M = 240$ and different K, N combinations. The optimization is performed for two classes of pulses. The former class comprises pulses that have Hermitian symmetry so that the DFT coefficients are real (see (19)-(22)). These pulses can have real or complex impulse response depending on the spectrum symmetry. The latter class of pulses includes asymmetric pulses that have complex and asymmetric impulse and frequency response.

As baseline pulses, we consider the rect and the rrc (in the frequency domain) pulses an example of which is shown in Fig. 2. In the special case $K = N$, the baseline prototype pulse is rectangular, i.e. $G(i) = 1$ for $i \in \{0, \ldots, Q-1\}$ and zero otherwise.

In Tab. I, we report the in-band-to-out-of-band energy ratio for $K = 12, 20, 24$ and different N values. For $K = N$, the system exhibits the maximum transmission rate, equal to $R = 1/T$ symbols/s. In this case, the only Hermitian pulse is the baseline rectangular pulse. However, an asymmetric pulse (complex) exists and it increases the metric value by 1.5 dB. For $K < N$, the rate reduction allows the design of pulses that improve considerably the metric. We note that when the rate decrease, Hermitian and asymmetric pulses exhibit similar metric improvement.

In Fig. 3, we show an optimal prototype pulse example for $K = 12$ and $N = 16$ in discrete time. The pulses have complex impulse response.

In Fig. 4 and Fig. 5, we show the frequency response of the interpolated prototype pulses. In Fig. 4, we show the frequency response for $K = 12, N = 12$. For the baseline rectangular pulse, the frequency response decreases from -20 dB to -63 dB. For the optimal real DFT coefficients pulse, the frequency response is always below -40 dB and decreases to -60 dB. In Fig. 5, we show the frequency response for $K = 12, N = 16$. For the baseline pulse, the frequency response decreases from -30 dB to -58 dB. For the optimal real DFT coefficients pulse, the frequency response is always below -60 dB and decreases to -80 dB. For the optimal complex DFT coefficients pulse, the frequency response is always below -70 dB and it decreases to -100 dB showing a significant spectrum confinement.

TABLE I
In-band to out-band ratios for baseline and optimal pulses.

System Params.				Metric value (dB)		
K	N	Rate	Baseline	Base	Hermitian	Asym.
12	12	1.00	Rect	15.76	-	17.94
	16	0.75	RRC, $\beta = 0.34$	49.59	58.21	69.86
	20	0.60	RRC, $\beta = 0.67$	46.81	70.09	70.05
	24	0.5	RRC, $\beta = 1.00$	46.34	70.48	70.32
20	20	1.00	Rect	13.95	-	15.59
	24	0.83	RRC, $\beta = 0.20$	28.01	38.11	45.92
	30	0.67	RRC, $\beta = 0.50$	36.36	55.41	68.31
	40	0.5	RRC, $\beta = 1.00$	39.54	67.53	68.84
24	24	1.00	Rect	13.16	-	14.68
	30	0.80	RRC, $\beta = 0.25$	27.41	37.22	43.09
	40	0.60	RRC, $\beta = 0.67$	31.55	64.91	66.59
	48	0.50	RRC, $\beta = 1.00$	36.91	66.12	68.19

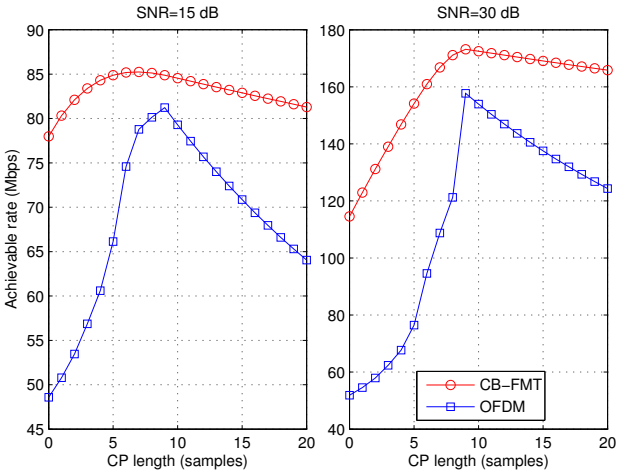

Fig. 6. Average maximum achievable rate for CB-FMT and OFDM as a function of the cyclic prefix length (in samples). For CB-FMT, the system parameters are $K = 24, N = 24, M = 240$. For OFDM, the sub-channel number is equal to $K = 32$. Both systems exploit a 1-tap equalizer.

An example of achievable performance is reported in Fig. 6. We consider both CB-FMT and OFDM. They both employ a cyclic prefix (CP) to cope with the channel dispersion and allow frequency domain equalization. For both systems, we use a 1-tap equalizer [12]. In particular, we show the average maximum achievable rate as a function of the CP length. For CB-FMT, we choose $K = 24, N = 24$ and the optimal pulse with length equal to $M = 240$ (critically sampled system). For OFDM, the number of sub-channels is equal to $K = 32$. The achievable rate is evaluated for an SNR equal to 15 and 30 dB. The achievable rate is averaged over different channel realizations (drawn randomly from a typical frequency selective Rayleigh fading channel model with exponential power delay profile, with delay spread equal to $0.15\mu s$ and bandwidth $1/T = 20$ MHz). The figure shows that CB-FMT offers higher achievable rate than OFDM. An optimal value of CP (shorter than the channel length) can be determined in both systems [19]. It should be noted that the rate decrease for CP lengths longer than the optimal value is lower for CB-FMT than for OFDM. Furthermore, CB-FMT offers much higher rate also in the absence of CP. The higher rate offered by CB-FMT than OFDM can be explained by its ability to better exploit the channel frequency diversity through FD equalization and the higher robustness to ICI and ISI due to the higher sub-channel frequency confinement with short duration pulses [10].

VI. Conclusions

In this paper we have investigated the optimal orthogonal design of a cyclic block FMT system. CB-FMT is a filter bank modulation scheme where linear convolutions are replaced by circular convolutions. We have shown that the orthogonal conditions can be written in the frequency domain allowing to derive simple hyper-spherical constraints for the pulse search. Furthermore, both real and complex impulse response pulses can be obtained with the objective of maximizing the in-band-to-out-of-band energy for maximum frequency confinement. Interestingly, a better than the trivial rectangular frequency domain window has been found which provides no rate loss, and about 1.5 dB gain in spectrum confinement. For lower spectral efficiency (rate below 1), both real and Hermitian impulse response pulses provide over 20 dB gain compared to rrc pulses.

References

[1] M. L. Doelz, E. T. Heald, and D. L. Martin, "Binary Data Transmission Techniques for Linear Systems," *Proceedings of the IRE*, pp. 656–661, 1957.

[2] J. A. C. Bingham, "Multicarrier Modulation for Data Transmission, an Idea whose Time Has Come," *IEEE Communication Magazine*, vol. 31, pp. 5–14, May 1990.

[3] IEEE, "802.11 Standard: Wireless LAN Medium Access Control and Physical Layer Specification," 2007.

[4] D. Astely, E. Dahlman, A. Furuskar, Y. Jading, M. Lindstrom, and S. Parkvall, "LTE: The Evolution of Mobile Broadband," *IEEE Communications Magazine*, vol. 47, no. 4, pp. 44–51, April 2009.

[5] Y. Mostofi and D. Cox, "Mathematical Analysis of the Impact of Timing Synchronization Errors on the Performance of an OFDM System," *IEEE Transactions on Communications*, vol. 54, no. 2, pp. 226–230, Feb 2006.

[6] Y. Li and L. Cimini, "Bounds on the Interchannel Interference of OFDM in Time-Varying Impairments," *IEEE Transactions on Communications*, vol. 49, no. 3, pp. 401–404, Mar 2001.

[7] H. Ochiai and H. Imai, "On the Distribution of the Peak-to-Average Power Ratio in OFDM Signals," *IEEE Transactions on Communications*, vol. 49, no. 2, pp. 282–289, Feb 2001.

[8] G. Cherubini, E. Eleftheriou, and S. Olcer, "Filtered Multitone Modulation for Very High-Speed Digital Subscribe Lines," *IEEE Journal on Selected Areas in Communications*, pp. 1016–1028, June 2002.

[9] P. Siohan, C. Siclet, and N. Lacaille, "Analysis and Design of OFDM/OQAM Systems Based on Filterbank Theory," *IEEE Transactions on Signal Processing*, vol. 50, no. 5, pp. 1170–1183, May 2002.

[10] A. M. Tonello, "A Novel Multi-carrier Scheme: Cyclic Block Filtered Multitone Modulation," in *Proc. of IEEE International Conference on Communications (ICC 2013)*, Budapest, Hungary, June 2013, pp. 3856–3860.

[11] ——, "Time Domain and Frequency Domain Implementations of FMT Modulation Architectures," in *Proc. of IEEE International Conference on Acoustics, Speech and Signal Processing (ICASSP 2006)*, vol. 4, May 2006, pp. IV–IV.

[12] A. M. Tonello and M. Girotto, "Cyclic Block Filtered Multitone Modulation," *EURASIP Journal on Advanced Signal Processing*, submitted to.

[13] C. Siclet, P. Siohan, and D. Pinchon, "Perfect Reconstruction Conditions and Design of Oversampled DFT-Modulated Transmultiplexers," *EURASIP Journal on Advances in Signal Processing*, vol. 2006, no. 1, 2006.

[14] N. Moret and A. M. Tonello, "Design of Orthogonal Filtered Multitone Modulation Systems and Comparison among Efficient Realizations," *EURASIP Journal on Advances in Signal Processing*, vol. 2010, no. 1, 2010.

[15] D. M. Y. Sommerville, *An Introduction to the Geometry of N Dimensions*. Methuen Publishin Ltd, 1929.

[16] R. H. Byrd, J. C. Gilbert, and J. Nocedal, "A Trust Region Method Based on Interior Point Techniques for Nonlinear Programming," *Mathematical Programming*, vol. 89, no. 1, pp. 149–185, 2000.

[17] R. H. Byrd, M. E. Hribar, and J. Nocedal, "An Interior Point Algorithm for Large-Scale Nonlinear Programming," *SIAM J. on Optimization*, vol. 9, no. 4, pp. 877–900, Apr. 1999.

[18] R. Waltz, J. Morales, J. Nocedal, and D. Orban, "An Interior Algorithm for Nonlinear Optimization that Combines Line Search and Trust Region Steps," *Mathematical Programming*, vol. 107, no. 3, pp. 391–408, 2006.

[19] A. M. Tonello, S. D'Alessandro, and L. Lampe, "Cyclic Prefix Design and Allocation in Bit-Loaded OFDM over Power Line Communication Channels," *IEEE Transactions on Communications*, vol. 58, no. 11, pp. 3265–3276, November 2010.